A silicon-based single-electron interferometer coupled to a fermionic sea

Anasua Chatterjee, Sergey N. Shevchenko, Sylvain Barraud, Rubén M. Otxoa, Franco Nori, John J. L. Morton, and M. Fernando Gonzalez-Zalba

Phys. Rev. B **97**, 045405 — Published 3 January 2018
DOI: 10.1103/PhysRevB.97.045405

A silicon-based single-electron interferometer coupled to a fermionic sea

Anasua Chatterjee,[1,*] Sergey N. Shevchenko,[2,3,4] Sylvain Barraud,[5] Rubén M. Otxoa,[6,7,8] Franco Nori,[2,9] John J. L. Morton,[1,10] and M. Fernando Gonzalez-Zalba[6,†]

[1] *London Centre for Nanotechnology, University College London, London, WC1H 0AH, United Kingdom*
[2] *Center for Emergent Matter Science, RIKEN, Wako-shi, Saitama 351-0198, Japan*
[3] *B. Verkin Institute for Low Temperature Physics and Engineering, Kharkov 61103, Ukraine*
[4] *V. Kazarin Kharkov National University, Kharkov 61022, Ukraine*
[5] *CEA/LETI-MINATEC, CEA-Grenoble, 38000 Grenoble, France*
[6] *Hitachi Cambridge Laboratory, J. J. Thomson Avenue, Cambridge CB3 0HE, United Kingdom*
[7] *Donostia International Physics Center, Donostia-San Sebastian 20018, Spain*
[8] *Department of Material Physics, Universidad del Pais Vasco, UPV/EHU, San Sebastian 20018, Spain*
[9] *Physics Department, University of Michigan, Ann Arbor, MI 48109-1040, USA*
[10] *Department of Electronic & Electrical Engineering, University College London, London WC1E 7JE, United Kingdom*

We study Landau-Zener-Stückelberg-Majorana (LZSM) interferometry under the influence of projective readout using a charge qubit tunnel-coupled to a fermionic sea. This allows us to characterise the coherent charge qubit dynamics in the strong-driving regime. The device is realised within a silicon complementary metal-oxide-semiconductor (CMOS) transistor. We first read out the charge state of the system in a continuous non-demolition manner by measuring the dispersive response of a high-frequency electrical resonator coupled to the quantum system via the gate. By performing multiple fast passages around the qubit avoided crossing, we observe a multi-passage LZSM interferometry pattern. At larger driving amplitudes, a projective measurement to an even-parity charge state is realised, showing a strong enhancement of the dispersive readout signal. At even larger driving amplitudes, two projective measurements are realised within the coherent evolution resulting in the disappearance of the interference pattern. Our results demonstrate a way to increase the state readout signal of coherent quantum systems and replicate single-electron analogues of optical interferometry within a CMOS transistor.

I. INTRODUCTION

Silicon quantum electronics is a nascent field in which the discreteness of the electron charge or spin is exploited to obtain additional device functionalities beyond the capabilities of the current silicon microelectronics industry [1]. Some of the most promising outcomes of this research field include: single-electron devices [2, 3] (performing logic operations at the device level [4], spin filters for spintronics [5], and aiming to redefine the Ampere [6]) and quantum computers and memories based on the long spin coherence times offered by silicon [7–10].

A developing area of silicon quantum electronics is the application of the coherent quantum properties of single-electron charge states to realise electronic analogues to optical interferometry experiments [11, 12]. Optical interferometry has enabled the development of extremely sensitive detectors that, for example, have recently detected gravitational waves [13]. However electron interferometry can lead to novel applications such as electron holography for precise imaging [14] or testing the effect of Fermi-Dirac statistics in quantum optics [15].

In quantum electronic devices, coupled two-level systems (TLS) can coherently split single electron states via Landau-Zener (LZ) transitions [16], with the quantum interference between consecutive LZ transitions giving rise to Landau-Zener-Stückelberg-Majorana interferometry (LZSM) [17]. This technique has been successfully applied to coherently control a variety of solid-state platforms such as superconducting qubits [18, 19], charge and spin qubits in semiconductor quantum dots and dopants [11, 20–22], and nitrogen vacancy centres in diamond [23], and has been used to address fundamental phenomena such as second-order phase transitions [24, 25].

In this Letter, we present an LZSM interferometry study performed in a single-electron double quantum dot (DQD) formed at the edge states of a silicon transistor fabricated using industry-standard 300 mm silicon-on-insulator technology [29]. The DQD operates in the charge qubit regime and is coupled to a fermionic sea, generating a multi-level energy spectrum. We readout the charge-qubit state dispersively, interfacing it with a high-frequency resonator via the gate [30, 31]. By tuning the microwave drive amplitude, we access multiple LZSM regimes, introducing increasing degrees of projective readout arising from the interaction with the fermionic reservoirs, which first enhance the interferometric signal, and then suppress it completely. Finally, we develop a theoretical model for the qubit-resonator interaction, accurately describing the interferometry and the dispersive signal enhancement. Our results motivate further studies exploring electron quantum optics in silicon and using the enhancement of the qubit readout signal for high-fidelity state readout.

* anasua.chatterjee@ucl.ac.uk
† mg507@cam.ac.uk

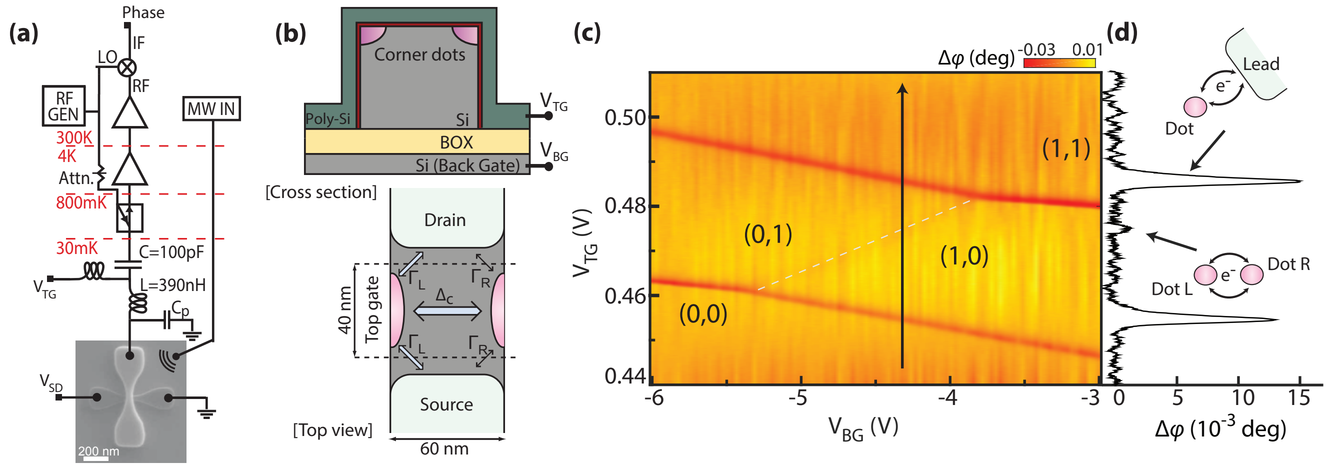

Figure 1. Dispersive detection of a DQD. (a) Scanning electron microscope image of a device connected to an RF-reflectometry setup via the top gate. A nearby on-PCB coplanar waveguide delivers MW signals. (b) Device schematic. Top: cross-section perpendicular to current flow direction, indicating the location of the corner QDs, where BOX indicates the buried oxide layer. Bottom: top-view of the device, with transparent top gate for clarity; five electronic transitions between dots and reservoirs marked by arrows. Δ_c represents the tunnel coupling and $\Gamma_{L(R)}$ the relaxation rates between the left(right) dot and the reservoirs. (c) Resonator phase response $\Delta\varphi$ as a function of top gate and back gate voltages (V_{TG}, V_{BG}). The white dashed line emphasizes the ICT and the black solid arrow indicates the position of the trace in panel (d). DQD electron numbers appear in parenthesis. (d) $\Delta\varphi$ as a function of V_{TG}, showing the relative intensity of the ICT and the DST.

II. DEVICE AND RESONATOR

We perform the experiment on a fully-depleted silicon-on-insulator nanowire transistor (height and width 11 nm and 60 nm, similar device shown in Fig.1(a) [32]). A 40 nm wide wrap-around top-gate (V_{TG}) covers the square-section channel, causing electron accumulation first at the topmost corners, creating a DQD in parallel with the source and drain, highly doped with arsenic [29, 33], see Fig.1(b). The silicon handle wafer constitutes a back-gate (V_{BG}). We perform gate-based radio-frequency reflectometry [12] in a dilution refrigerator (35 mK) using a tank circuit ($L = 390$ nH, parasitic capacitance $C_p = 660$ fF), and homodyne detection at resonance ($f_{rf} = 313$ MHz).

The demodulated phase response ($\Delta\varphi$) is sensitive to single-electron charge instability and more particularly to parametric capacitance changes (C_{pm}) occurring when electrons tunnel [34–38], with $\Delta\varphi = -\pi Q C_{pm}/C_p$, and Q the loaded Q-factor. We use this feature to measure the charge stability diagram in (V_{TG},V_{BG}) space in the subthreshold regime (Fig. 1(c)), indicating a few-electron DQD with four stable charge configurations (nm), where n and m refer to electron number. The absence of charge transitions at lower gate voltages indicates depletion of electrons. The device is operated as a single-electron charge qubit; an electron can occupy the left or right dot — states (10) and (01) — and unload or load an electron via the source and drain fermionic seas — states (00) and (11).

The DQD parametric capacitance seen from the top-gate is:

$$C_{pm} \approx -e\frac{\partial}{\partial V_{TG}}\left\{\alpha_L\langle n_L\rangle + \alpha_R\langle n_R\rangle\right\}, \qquad (1)$$

where $\alpha_{L(R)}$ represents the left (right) top-gate coupling and $\langle n_{L(R)}\rangle$ is the average electron occupation of the left (right) dot [12]. To include the fermionic reservoirs, we utilize the occupation probabilities of the four charge states (P_{nm}) [12]:

$$C_{pm} \approx 2e^2\alpha_-^2\frac{\partial}{\partial\varepsilon_0}\left\{P_{01} - P_{10} + \frac{\alpha_+}{\alpha_-}(P_{00} - P_{11})\right\}. \qquad (2)$$

Here, $\alpha_\pm = (\alpha_L \pm \alpha_R)/2$ and the energy detuning between dots $\varepsilon_0 = -2e\alpha_-(V_{TG} - V_{TG0})$, where V_{TG0} is the top-gate voltage at which (10) and (01) hybridize (depending on V_{BG}). In the common situation where the dots have similar top-gate couplings (i.e. small α_-), transitions involving (00) and (11) states yield α_+/α_- larger change in capacitance than those involving (01) and (10) states. Fig.1(d) shows this phenomenon, where the phase shift of dot-to-sea transitions (DST) is approximately 15 times larger than the interdot charge transition (ICT); in agreement with an independent magnetospectroscopy measurement of α_+/α_-=18 (see Supplementary Information [40]).

III. LZSM INTERFEROMETRY: MULTI-PASSAGE REGIME

Coherent LZSM interference occurs when a system is repeatedly (at least twice) driven through an anticrossing

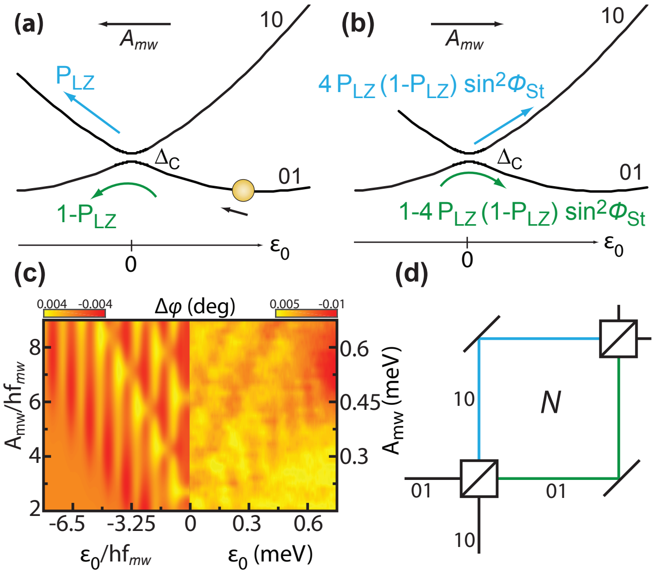

Figure 2. Multi-passage LZSM interferometry. Schematic of the probability distribution after the first (a) and second (b) passage. (c) $\Delta\varphi$ calculated (left of panel) vs experimental (right of panel), both panels mirrored in the horizontal direction with respect to one another. (d) Optical interferometry analogue showing the photon paths (electron charge states), the beam splitters (fast passage through the anticrossing) and refocusing mirrors (microwave electric fields). Here the process is repeated N times.

(of energy Δ_c) at a rate comparable to $(\Delta_c/h)^2$, and over timescales shorter than the coherence time T_2.

To perform coherent fast passages through the DQD anticrossing, a harmonic microwave electric field of amplitude A_{mw} and frequency $f_{mw} = 21$ GHz is delivered via an on-PCB antenna. This effectively varies, periodically, V_{TG} -and hence ε_0- at fixed V_{BG} (black line in Fig. 1(c)).

To model the coherent evolution, we use a full unitary description of each passage and the dynamical phase acquired (see [40]). To summarize, the probability, P_{LZ}, that an electron performs an LZ transition to the excited state following a passage is (Fig.2(a)):

$$P_{LZ} = \exp\left(-\frac{\pi\Delta_c^2}{2hf_{mw}\sqrt{A_{mw}^2 - \varepsilon_0^2}}\right). \tag{3}$$

Starting in state (01), after two passages, the probability of returning to (01)—Fig.2(b)—is:

$$P_{LZ,2} = 1 - 4P_{LZ}(1 - P_{LZ})\sin^2\phi_{St}, \tag{4}$$

where the Stückelberg phase $\phi_{St} = \phi_{St}(\varepsilon_0, f_{mw}, A_{mw})$ captures the phase difference acquired during free evolution. If the charge coherence is preserved for even longer timescales, multiple correlated passages lead to a stationary probability distribution in P_{01}:

$$P_{LZ,N} = \frac{1}{2}\left[1 + \mathrm{sgn}(\varepsilon_0)(1 - 2P_{LZ,N}^+)\right], \tag{5}$$

$$P_{LZ,N}^+ = \frac{1}{2}\sum_k \frac{\Delta_{c,k}^2}{\Delta_{c,k}^2 + \frac{T_2}{T_1}(|\varepsilon_0| - khf_{mw})^2 + \frac{\hbar^2}{T_1T_2}}, \tag{6}$$

with charge relaxation time T_1, $\Delta_{c,k} = \Delta_c J_k(A_{mw}/hf_{mw})$ and J_k the Bessel function of the k^{th} order. This detuning-dependent probability can be converted to a capacitance using Eq. (2). Assuming A_{mw} is not large enough to reach the crossings with the (00) and (11) states ($P_{00} = P_{11} = 0$), we obtain C_{pm} in the multi-passage regime:

$$C_{pm} \simeq 4e^2\alpha_-^2 \frac{\partial}{\partial\varepsilon_0}P_{01} \quad \text{and} \quad P_{01} = P_{LZ,N}. \tag{7}$$

Both measured and calculated interferometry patterns in Fig. 2(c) show the signatures of multi-passage LZSM: enhanced $\Delta\varphi$ at equally-spaced points in ε_0, separated by the photon energy hf_{mw}, and (quasi)periodic $\Delta\varphi$ oscillations for increasing A_{mw}. The interference pattern disappears for $f_{mw} < 4$ GHz, indicating that $T_2 \sim 0.25$ ns (see [40]). Since we use a classical resonator ($f_{rf} \ll k_BT/h, f_{mw}$), the probabilities appear stationary and Eq. (7) holds. In our simulations, we use $\Delta_c = 34$ μeV (extracted from the FWHM of the ICT), $T_2 = 0.25$ ns, and find the best fitting T_1 for $T_1 = 5T_2 = 1.25$ ns.

The electron manipulation resembles a multi-passage Mach-Zehnder interferometer (Fig. 2(d)) with the role of the beam-splitter played by the anticrossing splitting the electronic wavefunction [20], and the phase difference is here ϕ_{St}. The microwave drive refocuses the electron paths, repeating $N = T_2 f_{mw} \approx 5$ times. These results demonstrate that, although continuously monitoring the qubit state, the non-demolition nature of gate-based readout does not preclude multiple coherent passages.

IV. LZSM INTERFEROMETRY WITH PROJECTIVE READOUT

For larger driving fields (A_{mw}) or detunings (ε_0) transitions to the (00) and (11) states come into play. Firstly, these transitions involve charge transfer into a fermionic sea (not phase-preserving), introducing projective readout of the charge. Secondly, as discussed, DSTs yield a much larger reflectometry signal $\Delta\varphi$ than for qubit states (01) and (10).

To understand the coherent evolution through the charge configurations, in Fig. 3(a) we calculate the full DQD energy-level spectrum versus reduced detuning ε_0/E_C — where E_C is the charging energy — for top-gate coupling asymmetry $\alpha_- = 0.05$ (see [40]). Additionally, in Fig. 3(b), we measure $\Delta\varphi$ as a function of ε_0 and A_{mw} across a large range (of which Fig. 2(c) is a subset),

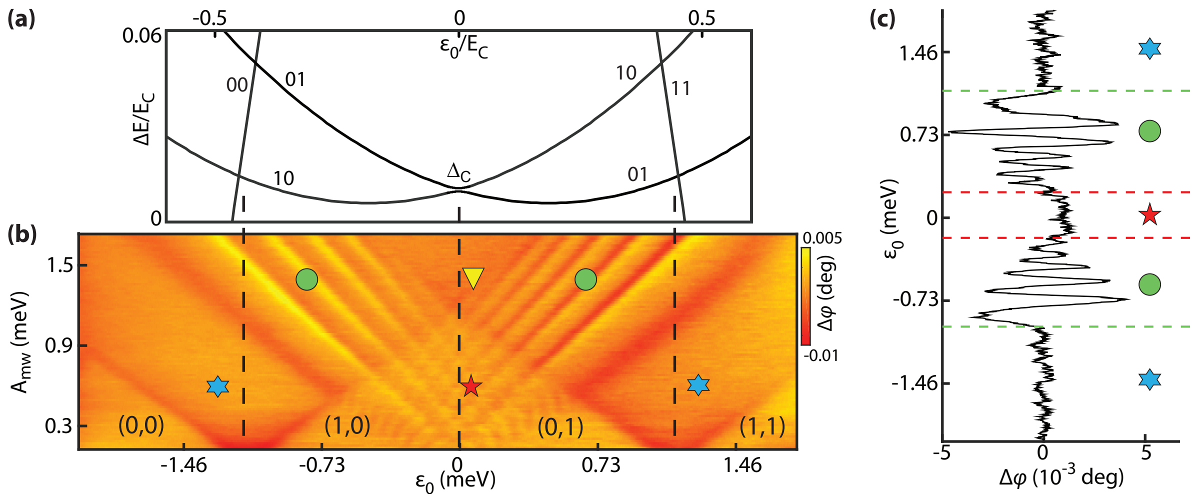

Figure 3. Multi-level LZSM interferometry. (a) Calculated DQD energy level diagram as a function of reduced detuning $\varepsilon_0/E_\mathrm{C}$; α_-=0.05 and $E_\mathrm{m}/E_\mathrm{C} = 10$, where E_m is the mutual charging energy. (b) $\Delta\varphi$ measured as a function of the detuning, ε_0, and MW amplitude, A_mw, for $f_\mathrm{mw} = 21$ GHz. Regions of constant $\Delta\varphi$, with well-defined electron numbers, are indicated in parenthesis. The (10)-(01) anticrossing, and the (00)-(10) and (01)-(11) crossings are indicated by black dashed lines. Incoherent, multi-passage, double-passage and single-passage LZSM regions are indicated by the blue star, red star, green circle and yellow triangle respectively. (c) $\Delta\varphi$ vs ε_0 trace at $A_\mathrm{mw} = 0.55$ meV and $f_\mathrm{mw} = 11$ GHz. Symbols as in (b).

enabling LZSM interferometry involving the four DQD charge states. For small A_mw, we label charge-stable regions (constant $\Delta\varphi$). Elsewhere, charge transitions occur, leading, in some cases, to interferometric patterns. We identify four distinct LZSM regimes, three involving passages through the ICT, which we indicate by the symbols in Fig. 3(b).

For small A_mw and ε_0 (red star), multipassage LZSM interference occurs, as explained above. As A_mw and ε_0 are increased, the DSTs are crossed, producing, a double-passage LZSM interference pattern where projective readout via the (00) and (11) states is performed every second passage (green circle). Due to the DST, the interference pattern amplitude in this regime is as much as 8 times greater than in the multipassage region. This is illustrated in Fig. 3(c), where we plot $\Delta\varphi$ against ε_0 for $A_\mathrm{mw} = 0.55$ meV and $f_\mathrm{mw} = 11$ GHz. For yet larger values of A_mw, while ε_0 remains small, projective readout occurs after every passage, making the interference pattern disappear (yellow triangle). Finally, though outside the scope of this Letter, we highlight regions (blue star) where DST-mediated incoherent LZSM occurs, see [40].

A. Double-passage regime

We move on to the double-passage regime in Fig. 3(b). Following a microwave-driven double-passage over the anticrossing, Eq. (4) gives the (01) and (10) state probability distribution. Due to the larger microwave amplitude, the system encounters DSTs where both (01) and (10) states cross (e.g.) the (11) state (Fig. 4(a,b)).

To understand the charge dynamics, we require insights into the dot-reservoir relaxation rates. We estimate the right dot-reservoir rate, $\Gamma_\mathrm{R} < 12$ GHz, from the temperature dependence of the (10)↔(11) DST FWHM (see [40]). By analyzing the decay of the $\Delta\varphi$ oscillations towards low ε_0 (Fig. 3(c)), we extract a left dot relaxation rate $\Gamma_\mathrm{L} \approx 50$ GHz [40]. The relaxation rate ratio $\Gamma_\mathrm{R}/\Gamma_\mathrm{L} < 0.25$ indicates much faster relaxation via the left dot. This relaxation-rate asymmetry, combined with the small difference in ε_0 between the (10)↔(11) and (01)↔(11) DSTs, results in relaxation occurring primarily via the left dot after the double-passage. This projects the system into the (11) or (00) state, with subsequent passages through the anticrossing being uncorrelated.

To confirm this description, Fig. 4(c) presents the data alongside a simulation based on Eq. (2). Although here $P_{01}, P_{10}, P_{11} \neq 0$, the main contribution to the capacitance arises from P_{11}, due to the large α_+/α_-

$$C_\mathrm{pm} \approx 2e^2\alpha_-\alpha_+\frac{\partial}{\partial\varepsilon_0}P_{11}. \tag{8}$$

In the limit where $A_\mathrm{mw} \gg hf_\mathrm{mw}$ and ε_0 is close to the (01)↔(11) crossing, Eq. (8) becomes

$$C_\mathrm{pm} \approx 2e^2\alpha_-\alpha_+\frac{\Gamma_\mathrm{L}-\Gamma_\mathrm{R}}{2f_\mathrm{mw}}\frac{\partial}{\partial\varepsilon_0}P_{\mathrm{LZ},2}. \tag{9}$$

While both data and simulation show (quasi)periodic oscillations for increasing A_mw, as in the multi-passage regime, the periodic enhancement of $\Delta\varphi$ with ε_0 is absent, because only two consecutive passages are correlated [42]. Calculations are obtained using Eq. (9), considering leading terms in $\varepsilon_0/A_\mathrm{mw}$ for $P_{\mathrm{LZ},2}$ and with $\Delta_\mathrm{c} = 34$ μeV, $f_\mathrm{mw} = 21$ GHz. The good agreement shows the validity of this simple dynamical picture, demonstrating an efficient way to increase the dispersive readout signal after manipulation by projecting the coherent state

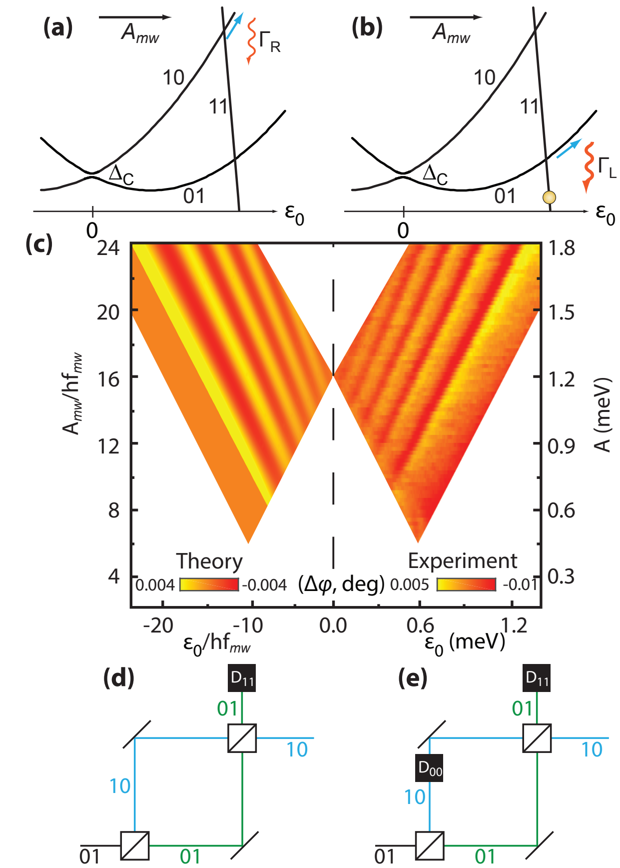

Figure 4. Double-passage LZSM interferometry. LZ transition schematic at the (10)-(11) (a) and (01)-(11) (b) crossings. The blue arrow indicates $P_{\rm LZ} \approx 1$ and the red arrow thickness shows the strength of the relaxation process. (c) $\Delta\varphi$ calculated (left) versus experimental (right, a section of Fig. 3(b)). (d) Optical interferometry analogue now including the detector D_{11} after the second passage [fast relaxation at the (01)-(11) transition]. (e) Optical interferometry analogue for the single-passage regime including an additional detector D_{00} after the first passage [relaxation at the (10)-(00) transition].

to an even-parity charge state. Comparing Eq. (7) and Eq. (9), we note the dispersive signal enhancement dependence on the amplification factor $\frac{\alpha_+}{\alpha_-}\frac{(\Gamma_{\rm L}-\Gamma_{\rm R})}{4f_{\rm mw}}$, and the key role of asymmetric relaxation rates in this dispersive detection mechanism. Finally, we observe that by performing a double-passage followed by a projective measurement, we can effectively control the coherence time, now determined by the MW period: $T_2 \sim f_{\rm mw}^{-1}$.

The electron evolution resembles a standard Mach-Zehnder interferometer. After a double-passage through the anticrossing, the (01) branch of the "beam" is detected via relaxation into the (11) state, indicated by the detector D_{11} for $\varepsilon_0 > 0$ (Fig. 4(d)). For $\varepsilon_0 < 0$, the (10) beam is read out by relaxation into the (00) state).

B. Single-passage regime

Finally, for large microwave driving amplitude centred around small detuning, the LZSM interference pattern disappears (Fig. 3(b), yellow triangle). The dynamic evolution now involves all four charge states. Every passage is followed by a projective measurement caused by electron tunnelling from the left dot to the source or drain. Without two consecutive passages with a phase coherent charge-state superposition, no interference signal manifests, even though the system is driven at $f_{\rm mw} = 21$ GHz, much faster than T_2.

Our optical analogue is again a standard Mach-Zenhder (Fig. 4(e)); however, now an additional detector or "observer" (D_{11} or D_{00}) is placed within one of the branches of the electron beam after the first beam splitter. This projective measurement collapses the charge superposition state after the first passage, and the interference pattern disappears.

V. OUTLOOK AND CONCLUSION

We have realised a multi-mode LZSM interference experiment in a CMOS transistor, observing the multiple-, double- and single-passage regimes of a single-electron charge qubit by adding progressive stages of projective readout. We have used additional levels arising from the interaction of the qubit with a fermionic reservoir to firstly project the coherent state of the qubit, enhancing the interferometric signal and secondly, suppressing the interference pattern completely. These observations raise possibilities of sophisticated coherent-control experiments using fast pulses for manipulation, followed by qubit readout via a dot-to-lead transition for enhanced signal. Our simulations, extending LZSM theory to a resonator-qubit coupled system, match our data well in each regime. In future, devices with additional tunability of the level couplings and the relaxation rates could provide access to even more complex interferometry experiments, opening a door towards silicon-based quantum optics.

ACKNOWLEDGMENTS

We thank A. J. Ferguson for discussions. We acknowledge the European Union's Horizon 2020 programme (grant agreement 688539, http://mos-quito.eu) and Seventh Framework Programme (FP7/2007-2013) (grant agreements 318397, http://www.tolop.eu, and 279781); as well as the Engineering and Physical Sciences Research Council through UNDEDD (EP/K025945/1). MFGZ acknowledges support from the Winton Programme for the Physics of Sustainability and Hughes Hall College (University of Cambridge). AC acknowledges support from the EPSRC Doctoral Prize Fellowship. FN was partially supported by the RIKEN iTHES Project, MURI Center for Dynamic Magneto-Optics via the AFOSR Award No. FA9550-14-1-0040, the Japan Society for the Promotion of Science (KAKENHI), the IMPACT program of JST, RIKEN-AIST "Challenge Research" program, JSPS-RFBR grant No 17-52-50023, CREST grant No. JPMJCR1676, and the Sir John Templeton Foundation. SNS was partially supported by the State Fund for Fundamental Research of Ukraine (F66/95-2016).

[1] F. A. Zwanenburg, A. S. Dzurak, A. Morello, M. Y. Simmons, L. C. L. Hollenberg, G. Klimeck, S. Rogge, S. N. Coppersmith, and M. A. Eriksson, "Silicon quantum electronics," Rev. Mod. Phys. **85**, 961–1019 (2013).

[2] A. Fujiwara and Y. Takahashi, "Manipulation of elementary charge in a silicon charge-coupled device," Nature **410**, 560–562 (2001).

[3] M. Fuechsle, J. A. Miwa, S. Mahapatra, H. Ryu, S. Lee, O. Warschkow, L. C. L. Hollenberg, G. Klimeck, and M. Y. Simmons, "A single-atom transistor," *Nat. Nano*, **7**, 242–246 (2012).

[4] J. A. Mol, J. Verduijn, R. D. Levine, F. Remacle, and S. Rogge, "Integrated logic circuits using single-atom transistors," *Proc. Nat. Acad. Sci.*, **108**, 13969–13972 (2011).

[5] B. Weber, Y. H. M. Tan, S. Mahapatra, T. F. Watson, H. Ryu, R. Rahman, Hollenberg L. C. L. L., G. Klimeck, and M. Y. Simmons, "Spin blockade and exchange in Coulomb-confined silicon double quantum dots," Nat. Nano **9**, 430–435 (2014).

[6] A. Rossi, T. Tanttu, K. Y. Tan, I. Iisakka, R. Zhao, K. W. Chan, G. C. Tettamanzi, S. Rogge, A. S. Dzurak, and M. Mottonen, "An accurate single-electron pump based on a highly tunable silicon quantum dot," Nano Lett. **14**, 3405–3411 (2014).

[7] J. T. Muhonen, J. P. Dehollain, A. Laucht, F. E. Hudson, R. Kalra, T. Sekiguchi, K. M. Itoh, D. N. Jamieson, J. C. McCallum, A. S. Dzurak, and A. Morello, "Storing quantum information for 30 seconds in a nanoelectronic device," Nat. Nano **9**, 986–991 (2014).

[8] M. Veldhorst, J.C.C. Hwang, C.H. Yang, A.W. Leenstra, B. de Ronde, J. P. Dehollain, J.T. Muhonen, F.E. Hudson, K.M. Itoh, A. Morello, and A. S. Dzurak, "An addresable quantum dot qubit with fault-tolerant controlfidelity," Nature **9**, 981–985 (2014).

[9] M. Veldhorst, C. H. Yang, J. C. C. Hwang, W. Huang, J. P. Dehollain, J. T. Muhonen, S. Simmons, A. Laucht, F. E. Hudson, K. M. Itoh, A. Morello, and A. S. Dzurak, "A two-qubit logic gate in silicon," Nature **526**, 410–414 (2015).

[10] M. Steger, K. Saeedi, M. L. W. Thewalt, J. J. L. Morton, H. Riemann, N. V. Abrosimov, P. Becker, and H.-J. Pohl, "Quantum information storage for over 180 s using donor spins in a ^{28}Si semiconductor vacuum," *Science*, **336**, 1280–1283 (2012).

[11] E. Dupont-Ferrier, B. Roche, B. Voisin, X. Jehl, R. Wacquez, M. Vinet, M. Sanquer, and S. De Franceschi, "Coherent coupling of two dopants in a silicon nanowire probed by Landau-Zener-Stückelberg interferometry," Phys. Rev. Lett. **110**, 136802 (2013).

[12] M. F. Gonzalez-Zalba, S. N. Shevchenko, S. Barraud, J. R. Johansson, A. J. Ferguson, F. Nori, and A. C. Betz, "Gate-sensing coherent charge oscillations in a silicon field-effect transistor," Nano Lett. **16**, 1614 (2016).

[13] B. P. Abbott et al. (LIGO Scientific Collaboration and Virgo Collaboration), "Observation of gravitational waves from a binary black hole merger," Phys. Rev. Lett. **116**, 061102 (2016).

[14] T. Akashi, Y. Takahashi, T. Tanigaki, T. Shimakura, T. Kawasaki, T. Furutsu, T. Shinada, H. Muller, M. Haider, N. Osakabe, and A. Tonomura, "Aberration corrected 1.2-MV cold field-emission transmission electron microscope with a sub-50-pm resolution," Appl. Phys. Lett. **106**, 074101 (2015).

[15] E. Bocquillon, V. Freulon, F. D. Parmentier, J.-M. Berroir, B. Placais, C. Wahl, J. Rech, T. Jonckheere, T. Martin, C. Grenier, D. Ferraro, P. Degiovanni, and G. Feve, "Electron quantum optics in ballistic chiral conductors," Annalen der Physik **526**, 1–30 (2014).

[16] W. D. Oliver, Y. Yu, J. C. Lee, K. K. Berggren, L. S. Levitov, and T. P. Orlando, "Mach-Zehnder interferometry in a strongly driven superconducting qubit," Science **310**, 1653–1657 (2005).

[17] S.N. Shevchenko, S. Ashhab, and Franco Nori, "Landau-Zener-Stückelberg interferometry," Phys. Rep. **492**, 1 – 30 (2010).

[18] M. Sillanpää, T. Lehtinen, A. Paila, Y. Makhlin, and P. Hakonen, "Continuous-time monitoring of Landau-Zener interference in a Cooper-pair box," Phys. Rev. Lett. **96**, 187002 (2006).

[19] C. M. Wilson, G. Johansson, T. Duty, F. Persson, M. Sandberg, and P. Delsing, "Dressed relaxation and dephasing in a strongly driven two-level system," Phys. Rev. B **81**, 024520 (2010).

[20] J. R. Petta, H. Lu, and A. C. Gossard, "A coherent beam splitter for electronic spin states," Science **327**, 669–672 (2010).

[21] J. Stehlik, Y. Dovzhenko, J. R. Petta, J. R. Johansson, F. Nori, H. Lu, and A. C. Gossard, "Landau-Zener-Stückelberg interferometry of a single electron charge qubit," Phys. Rev. B **86**, 121303 (2012).

[22] F. Forster, G. Petersen, S. Manus, P. Hänggi, D. Schuh, W. Wegscheider, S. Kohler, and S. Ludwig, "Characterization of qubit dephasing by Landau-Zener-Stückelberg-Majorana interferometry," Phys. Rev. Lett. **112**, 116803 (2014).

[23] J. Zhou, P. Huang, Q. Zhang, Z. Wang, T. Tan, X. Xu, F. Shi, X. Rong, S. Ashhab, and J. Du, "Observation of time-domain Rabi oscillations in the Landau-Zener regime with a single electronic spin," Phys. Rev. Lett. **112**, 010503 (2014).

[24] X. Y. Xu, Y. J. Han, K. Sun, J. S. Xu, J. S. Tang, C. F. Li, and G. C. Guo, "Quantum simulation of Landau-Zener model dynamics supporting the Kibble-Zurek mechanism," Phys. Rev. Lett. **112**, 035701 (2014).

[25] M. Gong, X. Wen, G. Sun, D. W. Zhang, D. Lan, Y. Zhou, Y. Fan, Y. Liu, X. Tan, H. Yu, Y. Yu, S.-L. Zhu, S. Han, and P. Wu, "Simulating the Kibble-Zurek

mechanism of the Ising model with a superconducting qubit system," Sci. Rep. **6**, 22667 (2016).

[26] D. M. Berns, M. S. Rudner, S. O. Valenzuela, K. K. Berggren, W. D. Oliver, L. S. Levitov, and T. P. Orlando, "Amplitude spectroscopy of a solid-state artificial atom," Nature **455**, 51–57 (2008).

[27] J. Stehlik, M. D. Schroer, M. Z. Maialle, M. H. Degani, and J. R. Petta, "Extreme harmonic generation in electrically driven spin resonance," Phys. Rev. Lett. **112**, 227601 (2014).

[28] J. Stehlik, M. Z. Maialle, M. H. Degani, and J. R. Petta, "Role of multilevel Landau-Zener interference in extreme harmonic generation," Phys. Rev. B **94**, 075307 (2016).

[29] B. Voisin, V.-H. Nguyen, J. Renard, X. Jehl, S. Barraud, F. Triozon, M. Vinet, I. Duchemin, Y.-M. Niquet, S. de Franceschi, and M. Sanquer, "Few-electron edge-state quantum dots in a silicon nanowire field-effect transistor," Nano Lett. **14**, 2094 (2014).

[30] J. I. Colless, A. C. Mahoney, J. M. Hornibrook, A. C. Doherty, H. Lu, A. C. Gossard, and D. J. Reilly, "Dispersive readout of a few-electron double quantum dot with fast rf gate sensors," Phys. Rev. Lett. **110**, 046805 (2013).

[31] M. F. Gonzalez-Zalba, S. Barraud, A. J. Ferguson, and A. C. Betz, "Probing the limits of gate-based charge sensing," Nat. Commun. **6**, 6084 (2015).

[32] A. C. Betz, S. Barraud, Q. Wilmart, B. Placais, X. Jehl, M. Sanquer, and M. F. Gonzalez-Zalba, "High-frequency characterization of thermionic charge transport in silicon-on-insulator nanowire transistors," Appl. Phys. Lett. **104**, 043106 (2014).

[33] A. C. Betz, M. L. V. Tagliaferri, M. Vinet, M. Broström, M. Sanquer, A. J. Ferguson, and M. F. Gonzalez-Zalba, "Reconfigurable quadruple quantum dots in a silicon nanowire transistor," Appl. Phys. Lett. **108**, 203108 (2016).

[34] R. Mizuta, R. M. Otxoa, A. C. Betz, and M. F. Gonzalez-Zalba, "Quantum and tunneling capacitance in charge and spin qubits," Phys. Rev. B **95**, 045414 (2017).

[35] S. N. Shevchenko, S. Ashhab, and F. Nori, "Inverse Landau-Zener-Stückelberg problem for qubit-resonator systems," Phys. Rev. B **85**, 094502 (2012).

[36] S. N. Shevchenko, D. G. Rubanov, and F. Nori, "Delayed-response quantum back action in nanoelectromechanical systems," Phys. Rev. B **91**, 165422 (2015).

[37] M. D. LaHaye, J. Suh, P. M. Echternach, K. C. Schwab, and M. L. Roukes, "Nanomechanical measurements of a superconducting qubit," Nature **459**, 960–964 (2009).

[38] Y. Okazaki, I. Mahboob, K. Onomitsu, S. Sasaki, and H. Yamaguchi, "Gate-controlled electromechanical backaction induced by a quantum dot," Nat. Commun. **7**, 11132 (2016).

[39] H. Sellier, G. P. Lansbergen, J. Caro, S. Rogge, N. Collaert, I. Ferain, M. Jurczak, and S. Biesemans, "Subthreshold channels at the edges of nanoscale triple-gate silicon transistors," Appl. Phys. Lett. **90**, 3 (2007).

[40] See Supplementary Material .

[41] F. Persson, C. M. Wilson, M. Sandberg, and P. Delsing, "Fast readout of a single Cooper-pair box using its quantum capacitance," Phys. Rev. B **82**, 134533 (2010).

[42] D. M. Berns, W. D. Oliver, S. O. Valenzuela, A. V. Shytov, K. K. Berggren, L. S. Levitov, and T. P. Orlando, "Coherent quasiclassical dynamics of a persistent current qubit," Phys. Rev. Lett. **97**, 150502 (2006).

[43] A. C. Betz, R. Wacquez, M. Vinet, X. Jehl, A. L. Saraiva, M. Sanquer, A. J. Ferguson, and M. F. Gonzalez-Zalba, "Dispersively detected Pauli spin-blockade in a silicon nanowire field-effect transistor," Nano Lett. **15**, 4622–4627 (2015).